

UNIVERSIDADE DE SÃO PAULO

PUBLICAÇÕES

**INSTITUTO DE FÍSICA
CAIXA POSTAL 66318
05389-970 SÃO PAULO - SP
BRASIL**

IFUSP/P-1177

**THE PARAMETER SPACE STRUCTURE OF THE
KICKED LOGISTIC MAP AND ITS STABILITY**

Murilo S. Baptista, Iberê L. Caldas
Instituto de Física, Universidade de São Paulo

Outubro/1995

The Parameter Space Structure of the Kicked Logistic Map and its Stability

Murilo S. Baptista , Iberê L. Caldas

Abstract

In this paper, it is analyzed the three-dimension parameter space of the Kicked Logistic Map (KLM), which is the Logistic Map perturbed by periodic kicks with constant amplitude. In this space parameter, diagrams are numerically determined identifying the regions with finite attractors and their topology. For the identified periodic regions, isoperiodic diagrams are also computed. Examples of these diagrams are presented for fixed kick periods. Dynamical properties of the KLM are characterized by the forms observed in these diagrams. Furthermore, the considered map has different basins of attraction. Thus, for the kick period $t = 2$, an analytical analysis shows the coexistence of two basins of attraction. In addition, for this kick period, a stability diagram is presented for the period-two orbits, without iterating the KLM, reproducing the corresponding regions in the isoperiodic diagrams. Lastly, the coexistence of two basins, one for a periodic and another for a chaotic attractor, causes, in critical regions of the parameter space, the appearance of a type of crisis named transfer crisis.

1 Introduction

For the specific purpose of controlling chaos, different methods of perturbing a dynamical system can be applied, as small parameter perturbations [1], parametric perturbations [2], or additive terms [3] as considered in this work. Generally, these finite perturbations alter the dynamics of the unperturbed system. However, if this is not possible or convenient, a system can still be controlled by slightly changing the appropriate control parameter, as it was proposed by Ott-Grebogi-Yorke [1990]. Other methods to control chaos are mentioned in [1], [4], [5].

A broad variety of papers have considered unimodal maps, as the Logistic one, to study how a chaotic system depends on the control parameters [6]. Particularly, the value of a control parameter can be varied in a previously established sequence to induce attractors independent of the initial conditions [7]. Maps can be also modulated by an additive periodic forcing, sometimes creating different basins of attraction [8]. To identify the changes caused by the application of such perturbations, one can compute usual investigating tools, as bifurcation diagrams, for the perturbation parameter.

However, there are systems for which more than one parameter can be varied, or, as considered by Rössler [6], where one parameter is assuming two different values. In these cases one should try to make up a new kind of diagram, showing the values of the perturbed parameters and the effect these variations cause into the system.

Thus, two-dimensional diagrams were computed with the control parameter values on the axis and pixels with different colors showing the studied attractor properties or characteristics.

One of the most used investigating tools is the signal of the Lyapunov function (to represent the attractor topology), or the magnitude of this function to show the strength of the sensibility to initial conditions [9]. Another example is the indication of the period in the so called isoperiodic diagrams [10, 11].

In this paper we consider the Kicked Logistic Map (KLM) [12, 13], which is the Logistic Map perturbed by a sequence of kicks with a constant amplitude, q , and a period, t :

$$X_{n+1} = bX_n(1 - X_n) \pm q\delta_{n,t} \quad \begin{cases} \delta_{n,t} = 1 & \text{if } \frac{n}{t} \text{ is an integer} \\ \delta_{n,t} = 0 & \text{otherwise} \end{cases} \quad (1)$$

where

$$0 < X < 1 \quad (2)$$

The purpose of this paper is not only to address the control of the Logistic Map trajectories, but also to discuss the bidimensional parameter diagrams and stability analysis for the perturbed orbits described by the KLM. Thus, these tools are used to investigate, in the parameter space, phenomena such as creation of chaos, abrupt disruption of the attractor, crisis, and bifurcation scenarios.

In section 2 we consider the KLM, for $t = 3$, and present bidimensional parameter diagrams. $b \times q$, to discern regions of chaotic, periodic, and non finite attractors. In section 3 we show how the period p of the KLM orbits are related to the kick period. Moreover, an equation is derived to obtain these periodic orbits. Finally, in section 4, we studied the case with $t = 2$, to show the existence of more than one basin of attraction and to study their stability. As we showed [13], this coexistence of different basis of attraction is responsible for a new type of crisis called transfer crisis [14]. In this paper these basins are presented. Finally, discussion is given in section 5.

2 The Parameter Space Structure

As we can see in Eq.(1), we have three parameters, namely, q , b , and t . The first two, q and b , have a wide range to be varied, but t assumes only integer values.

For a fixed kick period t , the trajectories obtained from (1), by setting different values of the other two parameters, can be classified in three different ways: chaotic, non-chaotic, and non-finite attractor (in this last case Eq.(2) is not satisfied). To get a global view of these orbits, we made diagrams that show for each pair of values (p, q) the observed kind of motion, and, in addition, the period p of the periodic orbits.

In fact, instead of showing these characteristics in only one diagram, we made two kinds of diagrams: one to discern if the orbit is chaotic, periodic or non-finite, and the other one to show the most observed low-periods p . Comparisons of these two diagrams confirm the relevance of the shown periods. As mentioned before, this last one is named an isoperiodic diagram [10, 11].

The quantification of chaos and order is obtained by computing the Lyapunov exponent [9], for the kicked logistic map trajectories. This is computed from the following expression obtained from Eq.(1):

$$\lambda = \lim_{N \rightarrow \infty} \frac{1}{N} \sum_{n=1}^N \ln |b(1 - 2X_n)| \quad (3)$$

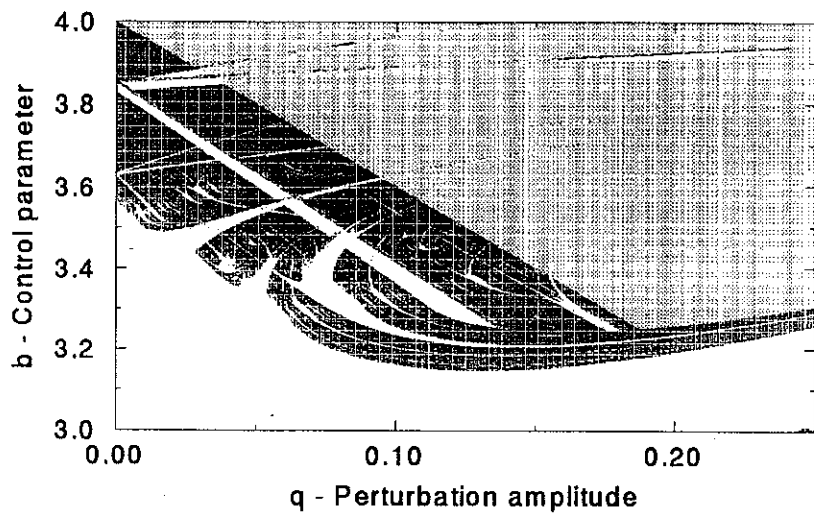


Figure 1: Attractor regions in the parameter space for kick period $t = 3$ with black and white pixels representing chaotic and non chaotic attractors. Gray pixels represent points without limited attractor.

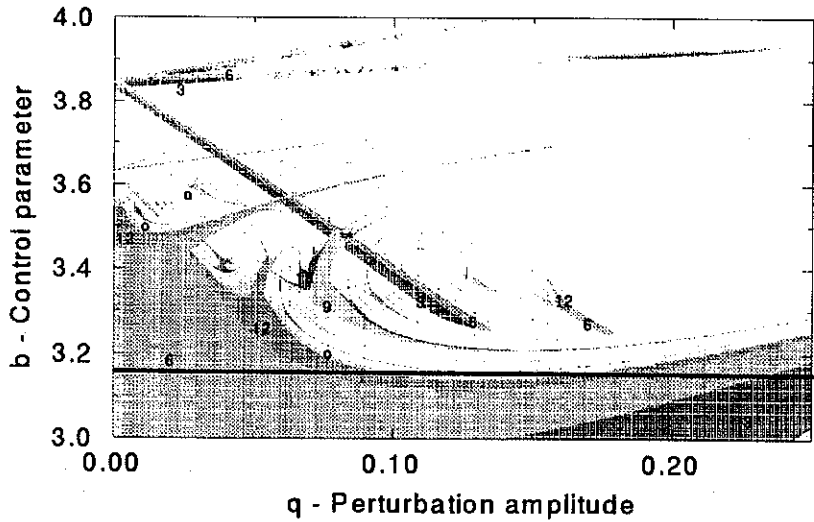


Figure 2: Isoperiodic diagram ($t = 3$) showing some of the periods p indicated by numbers and by the letter o for higher periods. Following the horizontal line we can get period doubling and inverse cascades.

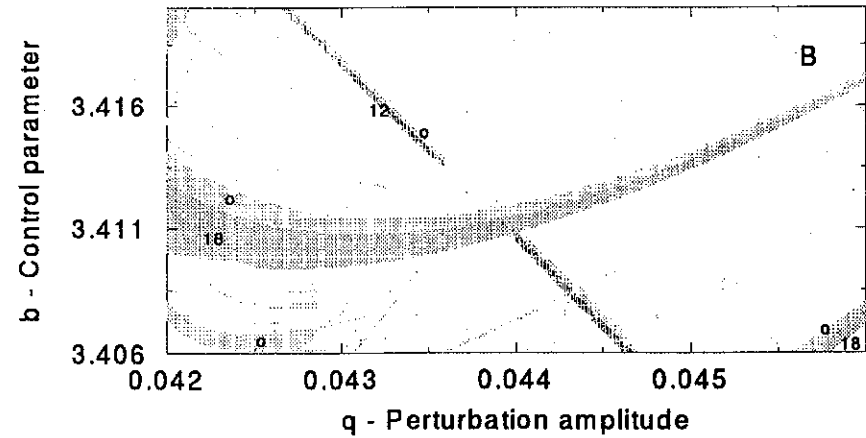
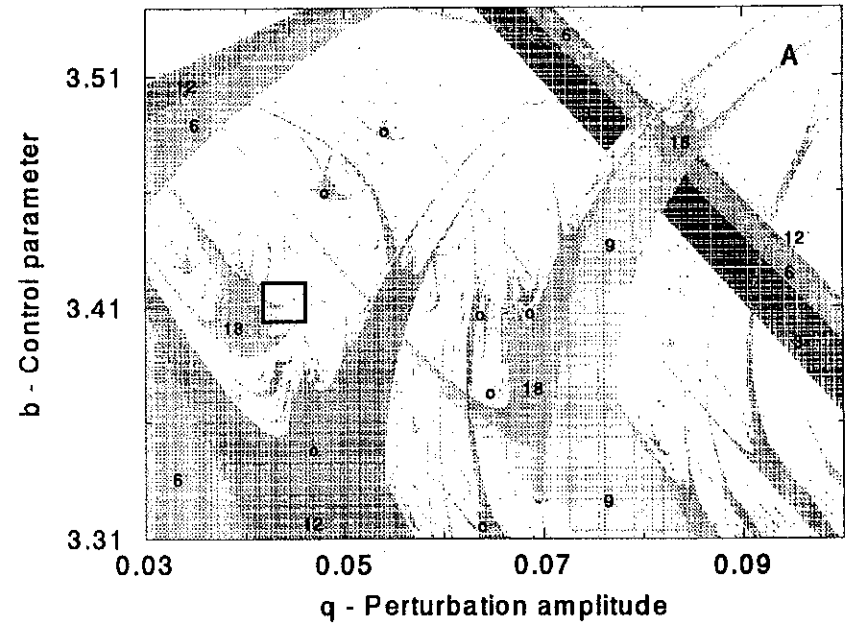


Figure 3: A) Magnification of the Fig. 2, showing some of the periods p indicated by numbers and by the letter o for higher periods. B) Magnification of the Fig. 3A, showing some of the periods p indicated by numbers and by the letter o for higher periods.

where X_n is obtained from Eq.(1). The order (i.e., predictability) is indicated by $\lambda < 0$, and the chaos (i.e., sensitive dependence on initial conditions) is indicated by $\lambda > 0$.

For each pair of values (b,q) , we iterate Eq.(1) and compute the Lyapunov exponent (considering 3000 iterations), after a transient of 1000 iterations. Much attention is paid to obtain highly precision figures. Thus, for parameters near critical values, as that corresponding to abrupt attractor changes or bifurcations, longer transients were considered (approximately 100000 iterations).

Then, setting the black color corresponding to chaotic attractors, the white to periodic ones, and the gray to non-limited ones, we obtain diagrams like that shown in Fig. 1. This diagram is obtained by setting $t = 3$ and the initial condition $X_0 = 0.2$. The computed regions are complex and highly interleaved. The figures obtained for other t values present similar patterns. In these diagrams, there is a basin of attraction for non finite attractors only for parameters satisfying the condition:

$$\frac{b}{4} + q > 1 \quad (4)$$

To identify the period of the Eq.(1), whenever we get a negative Lyapunov exponent, we keep one hundred iterations to find out the oscillation period, which is represented by pixels with different gray levels in the isoperiodic diagrams (Figs. 2, 3A, 3B).

Some important characteristics of these diagrams are the shrimp-shaped isoperiodic areas, which appear aligned along one direction, and a "structure-parallel-to-structure" of these areas. These results are similar to those reported for other non linear maps [10, 11]. Furthermore, the magnifications of Fig. 2 (see Fig. 3) show no structure-within-structure characteristic of fractal systems [9].

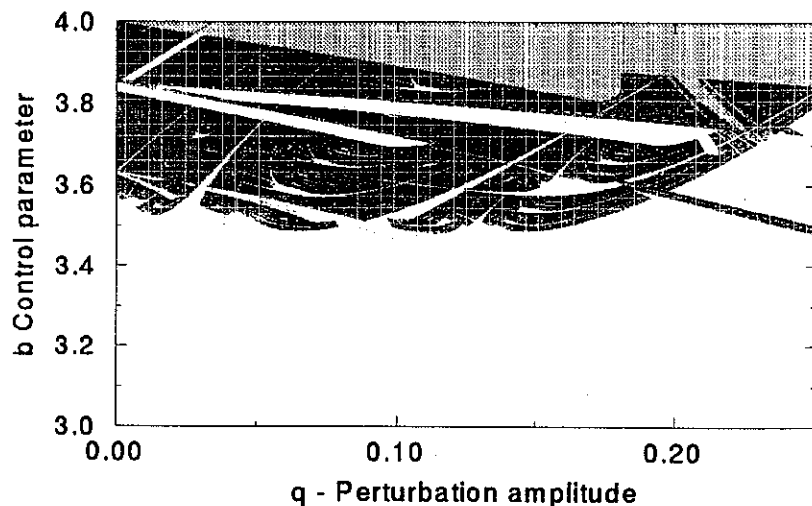


Figure 4: Attractor regions in the parameter space for kick period $t = 3$, and $q < 0$ with black and white pixels representing chaotic and non chaotic attractors. Gray pixels represent points without limited attractor.

In some experiences of control through impulsive perturbations it may be more convenient

to apply negative kicks [15, 16]. Therefore, Fig. 4 shows another space-parameter diagram for the same kick period, $t = 3$, and initial condition, $X_0 = 0.2$, but with subtracting perturbations, i.e., considering in the Eq.(1) a kick with amplitude $-q$. The main topological difference between this figure and Fig. 1 is that the basin of attraction for non finite attractors is given by the condition

$$\frac{b}{4} - q > 1. \quad (5)$$

Consequently, part of the chaotic region in Fig. 1 becomes periodic in Fig. 4, and part of the region without finite attractor in the first figure becomes chaotic in the last one.

The main period- p regions of the periodic regions of Fig. 4 are shown in the isoperiodic diagram of Fig. 5. Fig. 6 shows the magnification of the box showed in Fig. 5. Similarly to the observed in Fig. 3 for the positive kick, no structure-within-structure, characteristic of fractal systems [9], was observed.

All figures from 1 to 5 were made using the initial condition $X_0 = 0.2$. However, for different conditions we may not obtain the same diagram, since we have different basins of attraction for the system described by equation 1, as described in section 4.

3 The Trajectory Periods

From the isoperiodic diagrams showed in Figs. 2, 3, 5 and 6, we can get a global view of the sequences of the period-doubling and inverse cascades [17], as the b and q parameters change. Thus, the relevant critical attractor changes may be investigated in the appropriate bifurcation diagrams figured out from the corresponding roads observed in the computed isoperiodic diagrams

As an example, a bifurcation diagram could be made following the road indicated by the line in Fig. 2, for a fixed b and increasing q . Thus, in this diagram we would observe the following sequence of period- p orbits: 6,12,higher than 12,chaos,12,6,3. So, we get both, doubling and inverse cascades in the same diagram.

Another bifurcation diagram could be obtained by increasing b and fixing q , as it can be seen following the line in Fig. 5. Here the sequence of period- p orbits is: 3,6,12,higher than 12,chaos,9,18,chaos,3,12,...,6,12.

Though period doubling can be obtained by increasing either b or q , the same does not occur for inverse cascades obtained only by increasing q .

All the driven period- p orbits indicated in the previous isoperiodic diagrams are, in fact, multiple of t , with $p \geq t$. As a matter of fact, for any period- p orbit,

$$p = Nt, \quad \text{where } N=1,2,3,\dots, \quad (6)$$

there are other period- p' orbits that appear after m period-doubling bifurcations of the initially considered period- p orbit. Therefore, each sequence of periods p' given by the following equation

$$p' = 2^m p, \quad \text{where } m=1,2,3,\dots, \quad (7)$$

may describe a road to chaos.

These periodic orbits can be determined solving equations derived from (1). So, calling F as the first term of the right side of (1) (therefore F is the Logistic Map function), the equation that gives us a trajectory with period $p = t$ (given b and q) is:

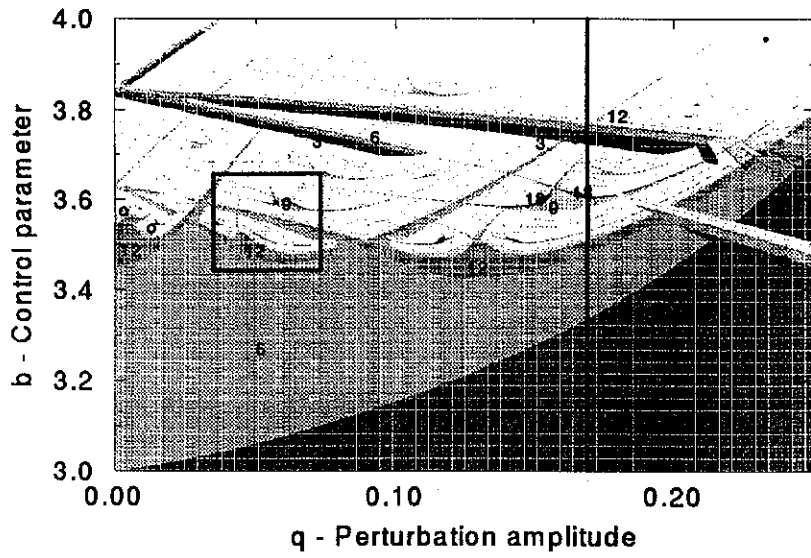


Figure 5: Isoperiodic diagram showing some of the periods p indicated by numbers and by the letter o for higher periods.

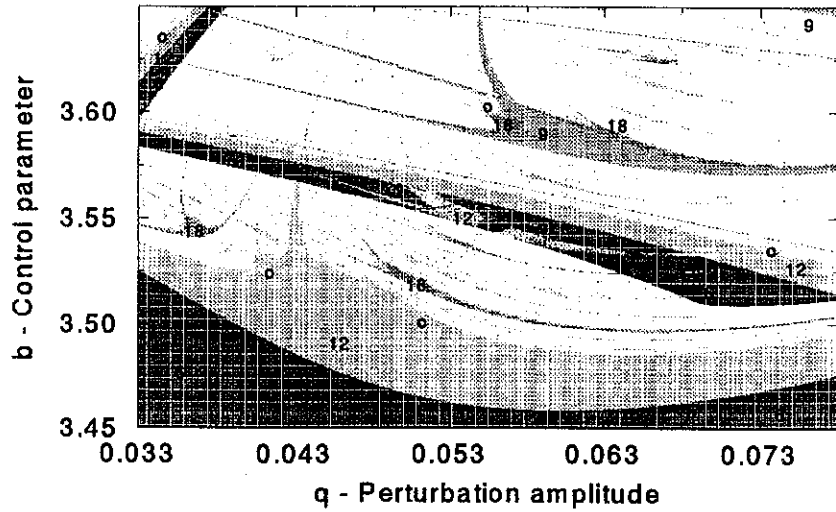


Figure 6: Magnification of a region of the Fig. 5 showing some of the periods p indicated by numbers and by the letter o for higher periods.

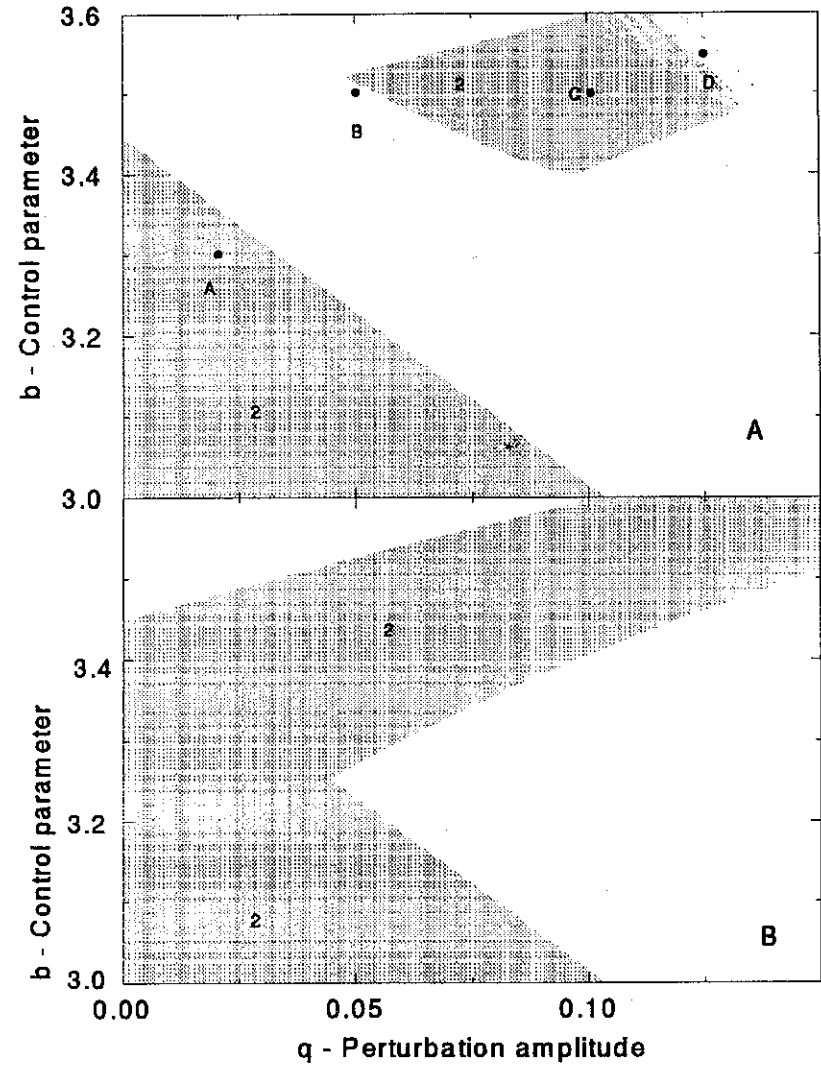


Figure 7: Isoperiodic diagram for $t = 2$ and $p = 2$. In (A) the initial condition is 0.3 and 0.5 in (B).

$$F^t(X_n) + q = X_n \quad (8)$$

where F^t is the t -th iteration of the function F . Similarly, the orbits with period $p = 2t$, can be determined from

$$F^t(F^t(X_n) + q) + q = X_n \quad (9)$$

The stability of the solutions obtained by these equations will be considered in the next section.

Thus, we could go further and write equations whose solutions would correspond to all periodic trajectories with $p = Nt$. Moreover, the solutions of these equations would be a 2^{Nt} order polynomial with period Nt .

4 Basins of Attraction and Stability

It was shown in the reference [13] that, for parameters satisfying the condition (4), there are basins of attraction for finite (either chaotic or periodic) and non limited attractors. Moreover, the regions shown in the isoperiodic diagrams may have also their own basins of attraction.

To show the existence of more than one basin of attraction, we analyzed the period-two regions in the isoperiodic diagrams of Figs. 2 and 3. The value $t = 2$ was chosen since we wanted to make an analytical study to compare with the results obtained by the iteration of equation (1), and this analysis would be difficult for periods higher than two.

Then, the period-two regions of two isoperiodic diagrams for different initial conditions $X_0 = 0.3$ and $X_0 = 0.5$ were computed (Fig. 7), showing that different diagrams can be obtained. The gray color is now used to indicated values of b and q that gives a period-two orbit ($p = 2$), of the equation (1), for $t = 2$.

To determine all possible period-two regions (for fixed b and q), without specifying the initial condition X_0 , we obtain from (8) the equation whose solutions give the periodic trajectories of (1) with $t = 2$:

$$F^2(X_n) + q = X_n \quad (10)$$

Therefore, with this equation, it is possible to obtain four real or complex period-two fixed points, X^{j*} , of (1). From (10), we get the following equation

$$-b^3 X^{j*4} + 2b^3 X^{j*3} - (b^3 + b^2) X^{j*2} + (b^2 - 1) X^{j*} + q = 0, \quad (11)$$

whose solutions correspond to the desired fixed points.

However, only the real and stable solutions of Eq. (11) are relevant to compute the isoperiodic diagrams. For a real fixed point X^{j*} to be stable, it must satisfy the following condition

$$\left| \frac{\partial F^2(X)}{\partial X} \Big|_{x=X^{j*}} \right| < 1. \quad (12)$$

In the case considered here, for $t = 2$, there may be none, one, or two stable fixed points (designated by X^{2*} and X^{4*}), depending on the control parameters b and q . With respect to the other two solutions, one (X^{1*}) does not satisfy condition (2), that is, it is in the basin of attraction of a non finite attractor. The other (X^{3*}) never satisfy condition (12), that is, it is always unstable as it can be seen in Figs. 9 - 12.

The existence of these stable values explains the existence of basins for the period-two attractors. So, Fig. 8 shows, for each par of parameters (b,q) , whether the fixed points, X^{2*} and X^{4*} , are stable or not. In this figure, the white regions correspond to (b,q) with no

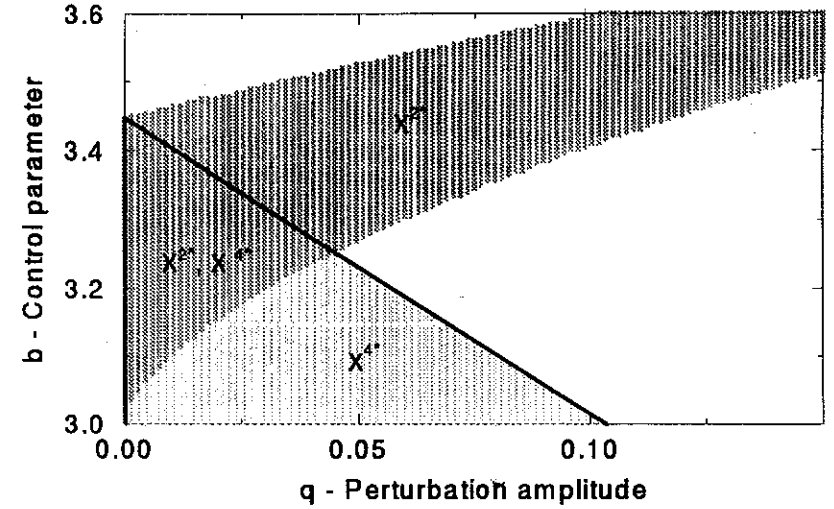


Figure 8: Stability regions of the period $p = 2$ fixed points X^{2*} and X^{4*} , in the parameter space, for $t = 2$.

period-two attractors. The gray regions correspond to (b,q) with one or two stable period-two attractors, as it is shown in the figure. All the period-two regions obtained in any isoperiodic diagram (for different initial conditions X_0), for $t = 2$, are within the gray regions of Fig. 8.

It is important to point out that the Fig. 7 was done by iterating (1) and verifying the period p of the obtained orbits, whereas Fig. 8 was done considering the stability of the fixed point of the map (1) by using equation (12).

Four points showed by the letters A,B,C,D in Fig. 7 were chosen to analyze the basins of attraction. For each of these points we studied their basins of attraction and the stability of the corresponding solutions of Eq.(11). To do that, we computed two kinds of figures (Figs. 9 to 12) introduced in the next paragraphs.

Each part A of Figs. 9 to 12 shows the dependence of three different functions on the position X . So, the dark black line represents the left side of Eq. (10), for each q and b chosen in Fig.7. Then, the straight gray line represents the identity function and the dashed line represents the left side of relation (10), that is, the derivative of the left side of Eq.(10) with respect to the position X . Furthermore, in the part A of these figures, the fixed points, X^{j*} , are localized by the crosses between the straight gray line and the dark black one. To verify if this fixed point X^{j*} is a stable or an unstable one, we look at the value of the function shown by the dashed line. Thus, it is possible to identify the period-two fixed points of Eq. (1) and their stability, that is, whether the condition (12) is satisfied or not.

Complementary, each part B of these figures represents the attractors of (1), for the same b and q considered in the part A, that is, the X_n values assumed by the orbits (after the transient) for each indicated initial condition X_0 . Thus, in these figures, it is possible to identify the

basins of attractions.

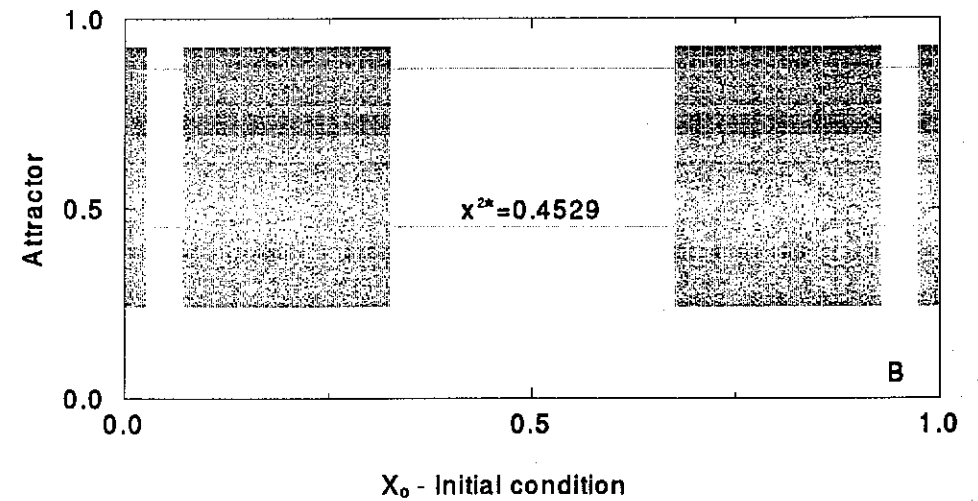
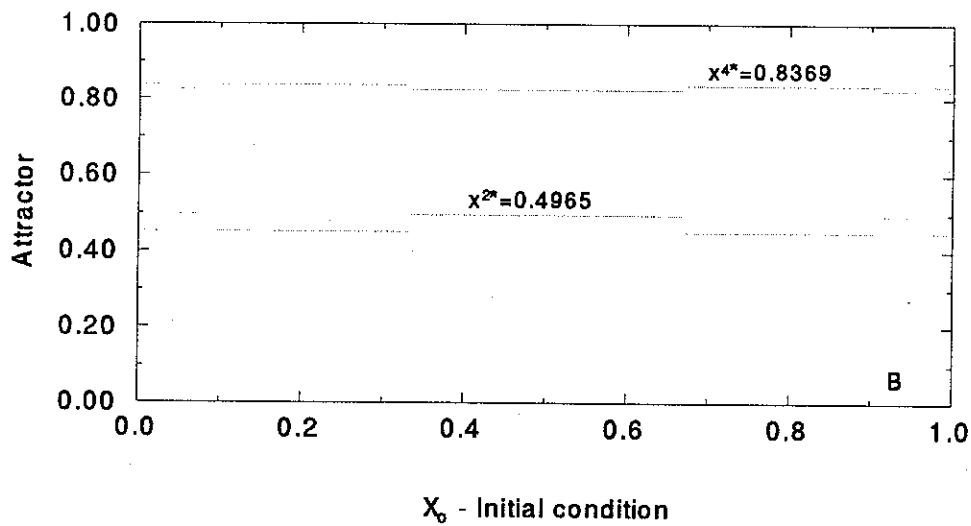
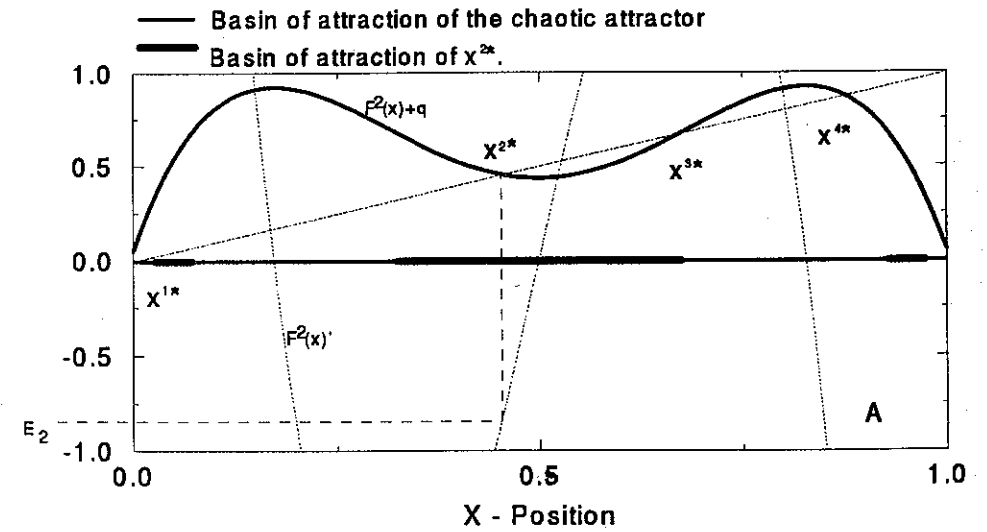
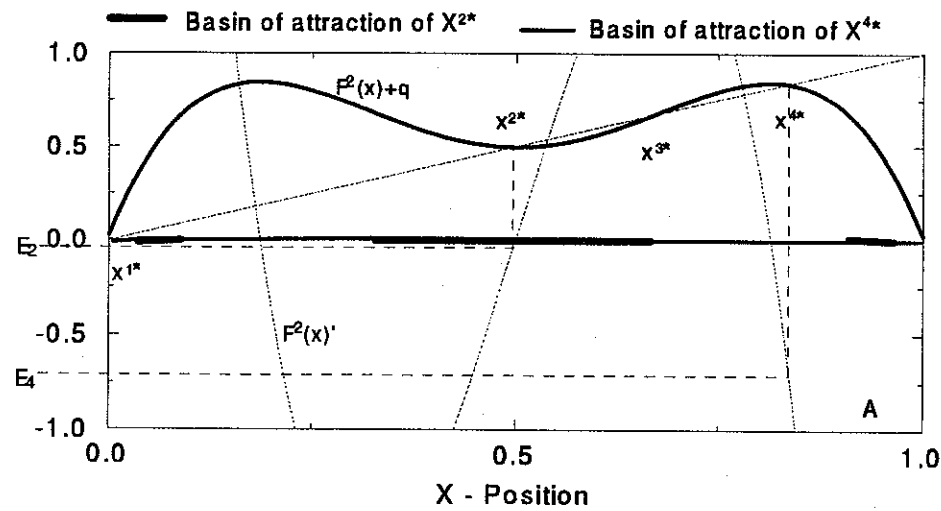


Figure 9: A) Graphical solution of Eq.(10), for $b = 3.3$ and $q = 0.02$, showing two stable fixed points and their basins of attraction. The function plotted with thin line represents the derivative of Eq.(10). B) KLM attractors with the same parameters of (A), for different initial conditions.

Figure 10: A) Graphical solution of Eq.(10), for $b = 3.5$ and $q = 0.05$, showing the fixed point X^{2*} and its basins of attraction. The function plotted with thin line represents the derivative of Eq.(10). B) KLM attractors with the same parameters of (A), for different initial conditions.

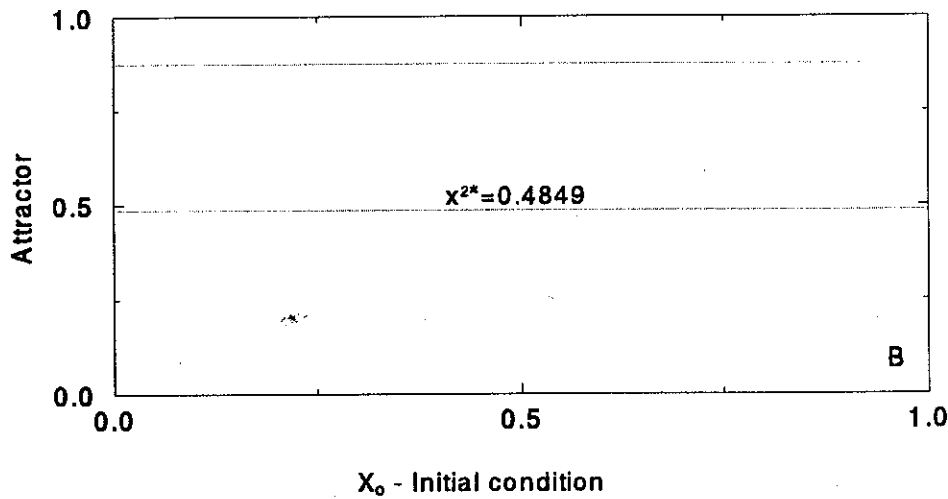
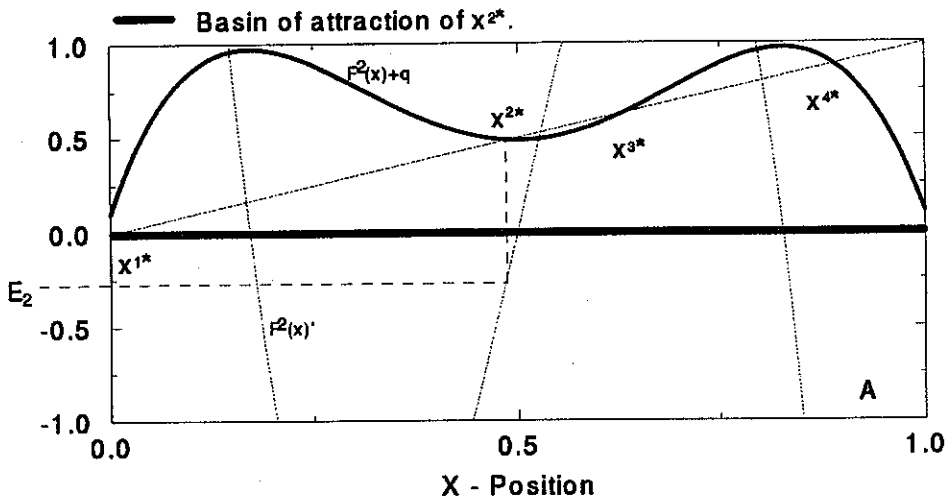


Figure 11: A) Graphical solution of Eq.(10), for $b = 3.5$ and $q = 0.1$, showing the stable point x^{2*} and its basin of attraction, which contains all initial condition (B).

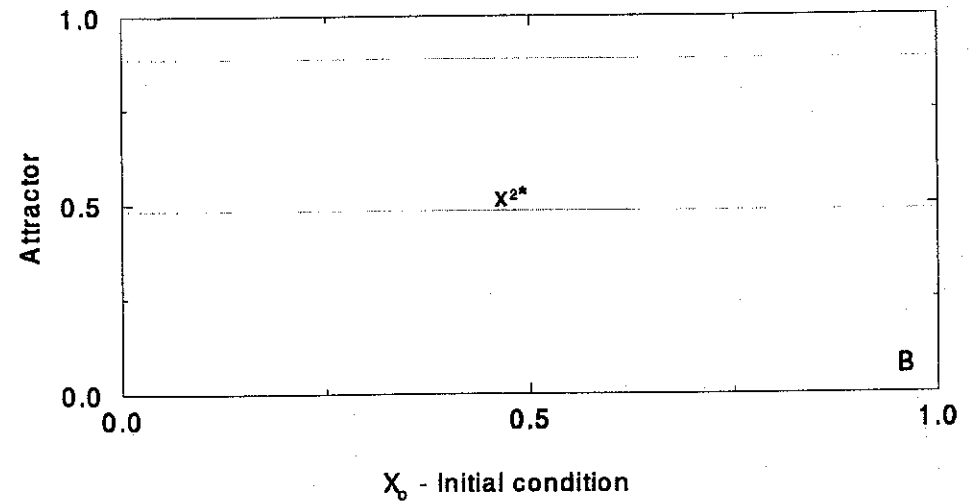
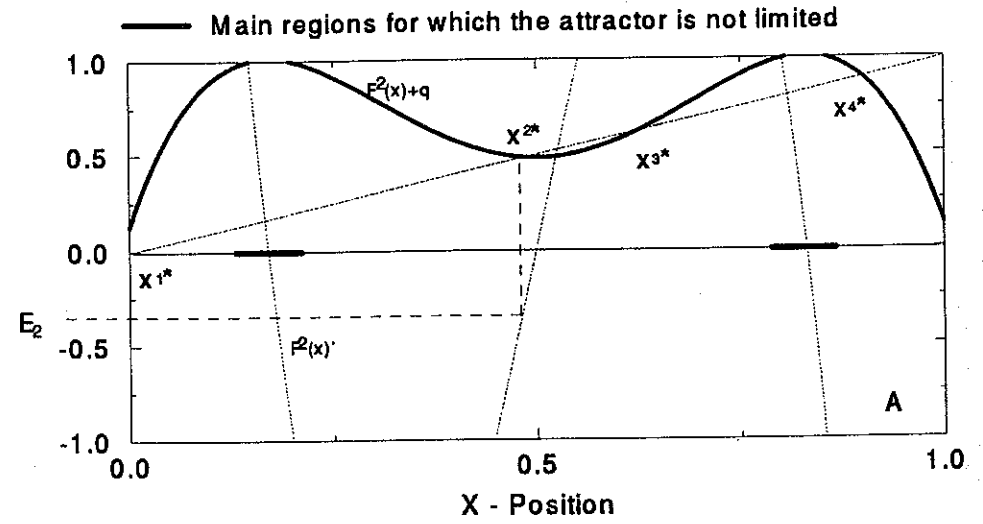


Figure 12: A) Graphical solution of Eq.(10), for $b = 3.55$ and $q = 0.125$, showing the main regions where the KLM is not limited. In (B), empty spaces correspond to initial conditions for which the attractor is not limited.

The KLM iterated for parameters corresponding to the point A in Fig. 7A has two period-two stable fixed points X^{2*} and X^{4*} indicated in Fig. 9A. In this figure, the basins of attraction of these two stable points can be identified by the huge black and black lines, respectively, that show the set of initial conditions whose orbits reach one of the two fixed points. The two X_n values assumed (after the transient) by the orbits associated to each fixed point can be seen, in Fig. 9B, for each initial conditions X_0 .

Similarly, for the point B, in Fig. 7A, we obtain Fig. 10 with only one period-two stable fixed point, X^{2*} . Here, however, there is also a chaotic attractor. The basins of these two attractors are shown in this figure, and the corresponding X_n values are shown in Fig. 10B.

The coexistence of these two basins of attraction may lead to transfer crises. This happens when, for increasing the control parameter b , the basin associated with the chaotic attractor became part of the basin associated with the periodic one. So, initial conditions, X_0 , initially in the basin associated with the chaotic attractor but very close to the edge between these two basins, goes to the basin of the periodic attractor. Thus, increasing b , chaotic attractors are suddenly transferred to periodic ones. This transfer crisis can be seen comparing bifurcation diagrams computed for b near the critical values [12, 13]. Thus, this crisis has characteristics different from other crises also observed in the KLM [13] or in other low-dimensional systems ([18], [19]).

By increasing b further, we can transfer all the chaotic attractors to periodic ones. This can be seen in Fig. 11, obtained for the point C in Fig. 7A. Accordingly, in this case, equation (1) is not dependent on initial conditions and there is only one stable attractor.

Finally, for the point D in Fig. 7A, there is only one stable periodic finite attractor, X^{2*} . However, here, since b and q satisfy the condition (4), there is also a non-finite attractor. Thus, Fig. 11 shows the basin of X^{2*} as well as X_0 intervals without finite attractor.

5 Conclusions

In this paper we considered the Kicked Logistic Map (KLM) [12, 13], which is the Logistic Map perturbed by a sequence of kicks with a constant amplitude, q , and a period, t . We presented a global view of how the KLM attractors depend on the control parameters, q , b , and t . To show that, we made two kinds of diagrams, obtained by varying the Logistic control parameter, b , and the kick amplitude, q , for each fixed discrete kick period t .

One kind of the presented diagrams show the periodic, chaotic, and the non finite attractor regions in the parameter space $b \times q$. These regions form complex and highly interleaved structures in the parameter space. As a matter of fact, fractal structure evidences were observed in broken bifurcation diagrams, that is diagrams with intervals without finite attractor.

The other kind of diagram shows, in the same $b \times q$ parameter space, the isoperiodic regions. Some important characteristics of these isoperiodic diagrams are the shrimp-shaped isoperiodic areas, which appear aligned along one direction, and a "structure-parallel-to-structure" of these areas. These results are similar to those reported for other unimodal two-parameter non linear maps [10, 11]. Furthermore, magnifications show no structure-within-structure characteristic of fractal systems [9].

From the isoperiodic diagrams we presented a global view of the sequences of the period-doubling and inverse cascades [17], as the b and q parameters change. Thus, the relevant critical attractor changes may be investigated in the appropriate bifurcation diagrams figured out from the corresponding roads observed in the computed isoperiodic diagrams. Though

period doubling can be obtained by increasing either b or q , the same does not occur for inverses cascades that are obtained only by increasing q .

The period- p fixed points, $p = Nt$ (N integer), could be determined by solving polynomial equations of order 2^{Nt} . The stability of these solutions can be determined from a condition obtained by linearizing the KLM in the fixed point neighborhoods. As an example, we solve the polynomial equation for $t = 2$ and determine the period-two stable regions in the parameter space $b \times q$. This result explains the shape of the $p=2$ regions obtained in the isoperiodic diagrams for that t value.

The KLM has basins of attraction of finite (either chaotic or periodic) and non limited attractors. The coexistence of two basins, one for a periodic and other for a chaotic attractor, can cause the appearance, in critical regions of the space parameter, of a type of crisis named transfer crisis [13, 14]. This happens when, varying the control parameter b , the basin associated with the chaotic attractor became part of the basin associated with the periodic one.

6 Acknowledgments

The authors would like to thank fruitful discussions with Prof. Dr. Celso Grebogi (The University of Maryland at College park), Prof. Dr. Ricardo L. Viana (Universidade Federal do Paraná), Dr. Jason A. C. Gallas and Prof. Thomas Braun (Universidade Federal do Rio Grande do Sul), and Dra. Mutsuko Y. Kucinski (Universidade de São Paulo). The computational assistance of Mr. W. P. de Sá is gratefully acknowledged. This work was partially supported by FAPESP and CNPq.

References

- [1] T. Shinbrot, C. Grebogi, E. Ott, J. A. Yorke, Nature **363**, 411 (1993). E. Ott, C. Grebogi, J.A. Yorke, Phys. Rev. Lett. **64**, 1196 (1990).
- [2] A.Y. Loskutov and A.I. Shishmarev, Chaos **4**, 391 (1994).
- [3] E.A. Jackson and A.Hübler, Physica D **44**, 407 (1990).
- [4] E. Ott, *Chaos in Dynamical Systems* (Cambridge University Press, Cambridge, 1993).
- [5] T. Kapitaniak, *Chaotic Oscillators* (World Scientific, Singapore, 1992).
- [6] J. Rössler, Phys. Rev. A **39**, 5954, (1989).
- [7] Sanju and V. S. Varma, Physical Review E **48**, 1670, (1993).
- [8] E. A. Jackson, Physica D **44**, 404 (1990).
- [9] P. Cvitanovic, *Universality in Chaos* (Adam Hilger, Bristol 1989).
- [10] J. A. C. Gallas, Phys. Rev. Lett., **70**, 2714 (1993).
- [11] J. A. C. Gallas, Physica A **202**, 196 (1994).
- [12] M. Baptista, I. L. Caldas, Proc. Int. Soc. Optical Engineering **2037**, 273 (1993).

- [13] M. Baptista, I.L. Caldas, *Dynamics of the Kicked Logistic Map*, Chaos, Solitons, and Fractals, to be published.
- [14] Y. Yamaguchi, K. Sakai, Phys. Rev. A **27**, 2755 (1983).
- [15] T. Braun, J.A. Lisboa, J.A.C. Gallas, Phys. Rev. Lett. **68**, 2770 (1992).
- [16] T. Braun, J. A. Lisboa, Int. J. of Bifurcations and Chaos, **4**, 1483 (1995).
- [17] S. P. Dawson, C. Grebogi, J. A. York, H. Hocak, Chaos, Solitons, and Fractals **1**, 137 (1991).
- [18] Y. Pomeau, P. Manneville, Commun. Math. Phys. **74**, 189 (1980).
- [19] C. Grebogi, E. Ott, J.A. Yorke, Phys. Rev. Lett. **48**, 1507 (1982).